The Antarctic Circumpolar Current in Three Dimensions

TIMOUR RADKO

Department of Oceanography, Naval Postgraduate School, Monterey, California

JOHN MARSHALL

Department of Earth, Atmospheric and Planetary Sciences, Massachusetts Institute of Technology, Cambridge, Massachusetts

(Manuscript received 4 June 2004, in final form 26 September 2005)

ABSTRACT

A simple theory is developed for the large-scale three-dimensional structure of the Antarctic Circumpolar Current and the upper cell of its overturning circulation. The model is based on a perturbation expansion about the zonal-average residual-mean model developed previously by Marshall and Radko. The problem is solved using the method of characteristics for idealized patterns of wind and buoyancy forcing constructed from observations. The equilibrium solutions found represent a balance between the Eulerian meridional overturning, eddy-induced circulation, and downstream advection by the mean flow. Depth and stratification of the model thermocline increase in the Atlantic–Indian Oceans sector where the mean wind stress is large. Residual circulation in the model is characterized by intensification of the overturning circulation in the Atlantic–Indian sector and reduction in strength in the Pacific Ocean region. Predicted three-dimensional patterns of stratification and residual circulation in the interior of the ACC are compared with observations.

1. Introduction

The absence of land barriers in the Antarctic Circumpolar Current (ACC) results in distinct dynamical features that have no direct counterpart in the theory of midlatitude ocean gyres. Sverdrup dynamics, the cornerstone of subtropical thermocline theory (Rhines and Young 1982; Luyten et al. 1983), do not apply here. Both wind and buoyancy forcing play a role, as do geostrophic eddies, which appear to be crucial in determining the stratification and transport of the ACC (see the review by Rintoul et al. 2001). The difficulty of incorporating eddy transfer led to a rather slow development of conceptual models of the ACC (see, e.g., Johnson and Bryden 1989; Marshall et al. 1993). Recently, however, residual-mean theories have been applied (see Karsten et al. 2002; Marshall and Radko 2003, MR hereinafter) that, we believe, capture the essence of the zonally averaged circulation and stratification of the Southern Ocean and fully embrace the central role of eddies. It is assumed that the Eulerian meridional circulation driven by the westerly winds (the Deacon cell), tending to overturn isopycnals, is largely balanced by the geostrophic eddies that act in the opposite sense. The transformed Eulerian-mean formalism (Andrews and McIntyre 1976) is used to represent the combined effect of eddy-induced and mean flow advection.

While the simplified two-dimensional zonal-average view attempts to explain the integral characteristics of the ACC, such as the overall strength of the overturning circulation and eastward baroclinic transport, zonal averaging masks important three-dimensional effects. For example, inspection of the pattern of the net surface heat flux in the Southern Ocean (Fig. 1) reveals its strikingly nonuniform distribution along the path of the ACC, with air–sea heat fluxes warming the ocean at rates reaching $\sim$60 W m^{-2} in the Atlantic and Indian Ocean sectors and becoming smaller and changing sign in the Pacific Ocean. The downstream variation in the surface forcing may be a consequence of the asymmetry in the trajectory of the ACC; the current is partially steered by bottom topography (Marshall 1995) and therefore does not exactly follow latitude circles. As a result, the surface heat flux into the ocean increases (relative to the streamline average) where the ACC meanders equatorward into warmer regions downstream of Drake Passage (see Fig. 1) and decreases when the ACC drifts poleward in the Pacific sector.

Corresponding author address: Timour Radko, Dept. of Oceanography, Naval Postgraduate School, Rm. SP-344, 833 Dyer Rd., Monterey, CA 93943.
E-mail: tradko@nps.edu

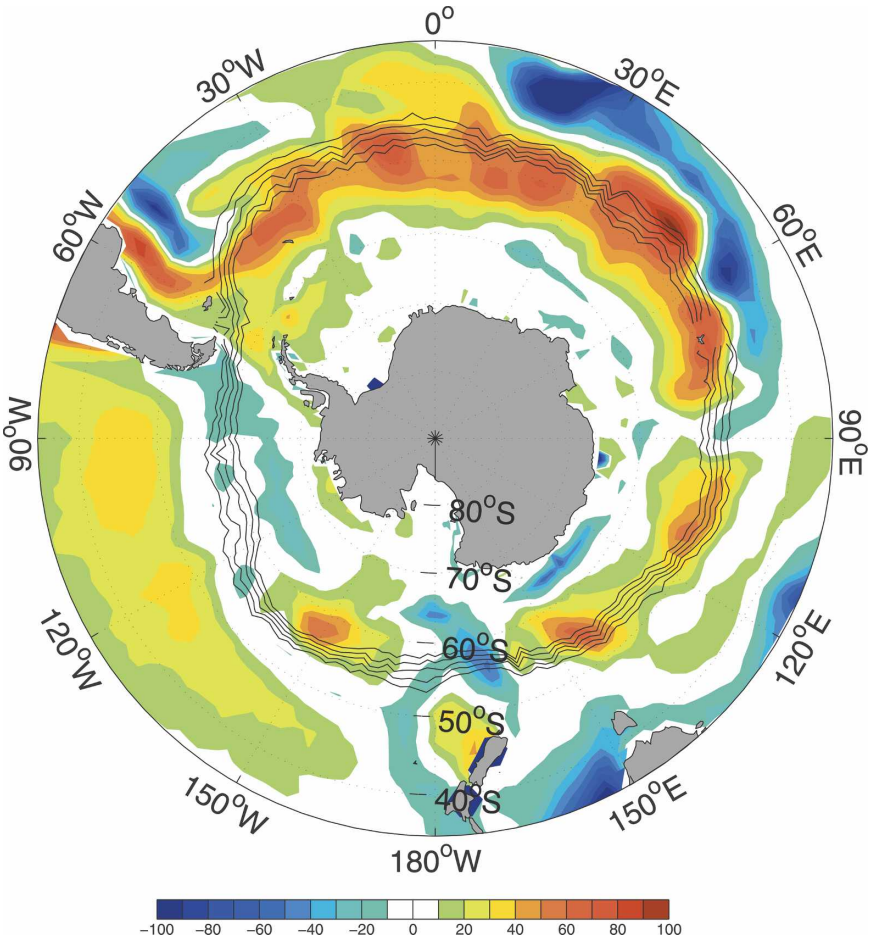

FIG. 1. Annual mean net surface heating of the ocean (W m^{-2}) estimated from the NCEP–NCAR reanalysis over 1980–2002 (A. Czaja 2004, personal communication). Superimposed are the sea surface height contours (contour interval = 10 cm) from satellite altimetry, which indicates the trajectory of the ACC.

Wind stress (Fig. 2a) also varies along the path of the ACC, being significantly larger in the Atlantic–Indian sector. In this paper we will argue that the spatially nonuniform forcing leads to downstream variation of the thermocline depth and stratification of the ACC [see observations of Sun and Watts (2002)] and modulates the strength of the upper cell of the meridional overturning circulation.

This study attempts to explain the three-dimensional time-mean structure of the ACC and the associated pattern of the overturning circulation by extending the zonal-average model of MR. Exploiting the asymptotic limit in which the downstream variation in buoyancy is assumed to be weak relative to its variation in the meridional plane, the problem is reduced to a system of equations that can be readily solved using the method of characteristics. The theory is analogous to linear models of forced stationary waves in the earth's troposphere [see the review by Held (1983)].

The paper is set out as follows. After presenting key observations of the ACC in section 2, we develop a theoretical framework (section 3) by introducing the quasi-zonal jet approximation. Residual-mean theory is used to incorporate the effects of mesoscale eddies. Simplifications introduced by the analytical model are then used to determine the interior structure of the ACC for various surface and boundary conditions. In section 4 we briefly consider the simplest "diagnostic" model, which involves prescribing the idealized distribution of the surface buoyancy (b_m), buoyancy flux (B), and wind stress (τ) and computing the resulting interior fields. In section 5 we study a different, and perhaps more physical, "prognostic" model in which the surface buoyancy distribution and fluxes are considered to be unknown and are computed as a part of the problem. Theoretical results are compared with the oceanographic observations. The physical interpretation of the model solutions (section 6) is accompanied by a

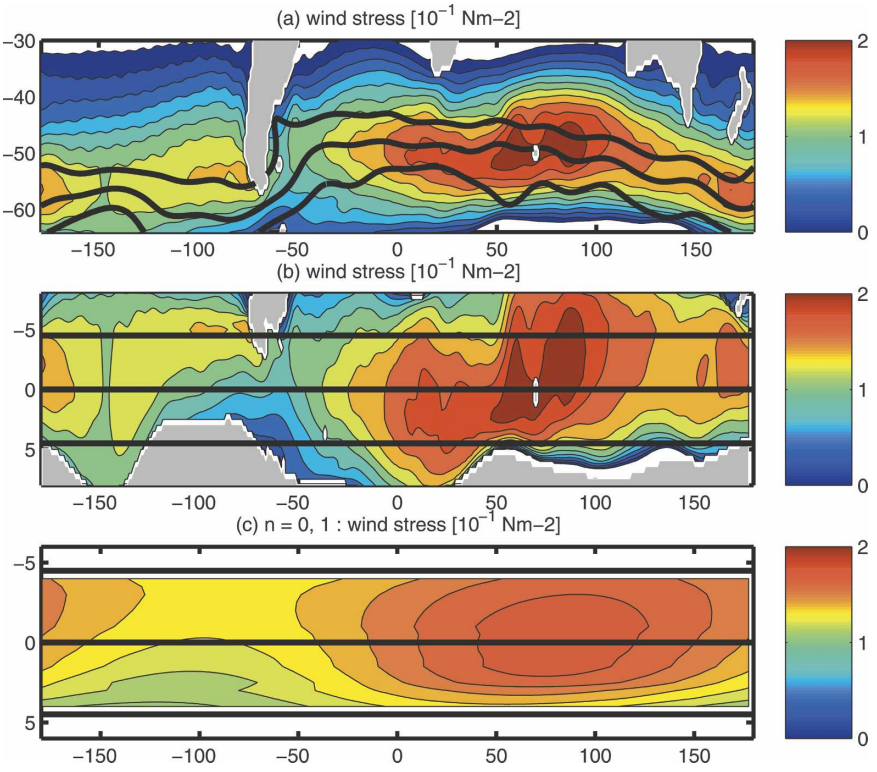

FIG. 2. Analysis of the observed (NCEP–NCAR) surface wind stress (T. Ito 2004, personal communication). (a) Zonal component of the wind stress. Heavy solid lines are the streamfunction contours obtained from the sea surface height that mark the boundaries and the axis of the ACC [$\Psi_g = -5, 0, 5$ ($\times 10^4$ m^2 s^{-1})]. (b) Projection of the data onto the frame of reference associated with the streamfunction; the curved streamlines in the top of the plot are now straight and horizontal. (c) The filtered data consisting of the two lowest Fourier components in x: the streamline average mode and the fundamental harmonic.

quantitative analysis of the buoyancy budget. We summarize and conclude in section 7.

2. Observational background

Figures 2–4 present key observations of surface properties and forcing of the Antarctic Circumpolar Current (to be used in our theoretical model). The pattern of zonal wind stress (τ) is shown in Fig. 2a, the surface buoyancy distribution (b_m) in Fig. 3a, and the air–sea buoyancy flux (B) in Fig. 4a.[1] To analyze the variation of these fields along the path of the ACC, it is convenient to reference our along-stream coordinate to mean surface geostrophic contours deduced from satellite altimetry; these are indicated by the heavy solid lines in Figs. 2a, 3a, and 4a, which mark the boundaries and the axis of the ACC. The width of the region bounded by these streamfunction contours is 1000–2000 km (depending on the longitude). Projection of the zonal wind stress, surface buoyancy, and buoyancy flux on to this coordinate system is shown in Figs. 2b, 3b, and 4b, respectively, where the ordinate is now a geostrophic streamline rather than latitude.

Several comments on the structure of the forcing fields are in order. Downstream (x) variation in (τ, B, b_m) contains a large signal in the fundamental (in x) harmonic whose wavelength equals the zonal extent of the ACC. The two lowest Fourier components in x—the along-stream average ($n = 0$ mode) mode and the fundamental harmonic ($n = 1$ mode)—capture much of the large-scale spatial variability of the ACC. Downstream variation in the wind stress (Fig. 2b) is rather moderate, about 20% of the mean. Winds over

[1] It should be noted that there is a significant uncertainty in the observations, particularly with regard to the air–sea fluxes; the estimates of the surface buoyancy flux from various datasets [e.g., the National Centers for Environmental Prediction–National Center for Atmospheric Research (NCEP–NCAR) reanalysis, Comprehensive Ocean–Atmosphere Dataset (COADS), and Southampton Oceanography Centre (SOC)] differ by as much as 50%.

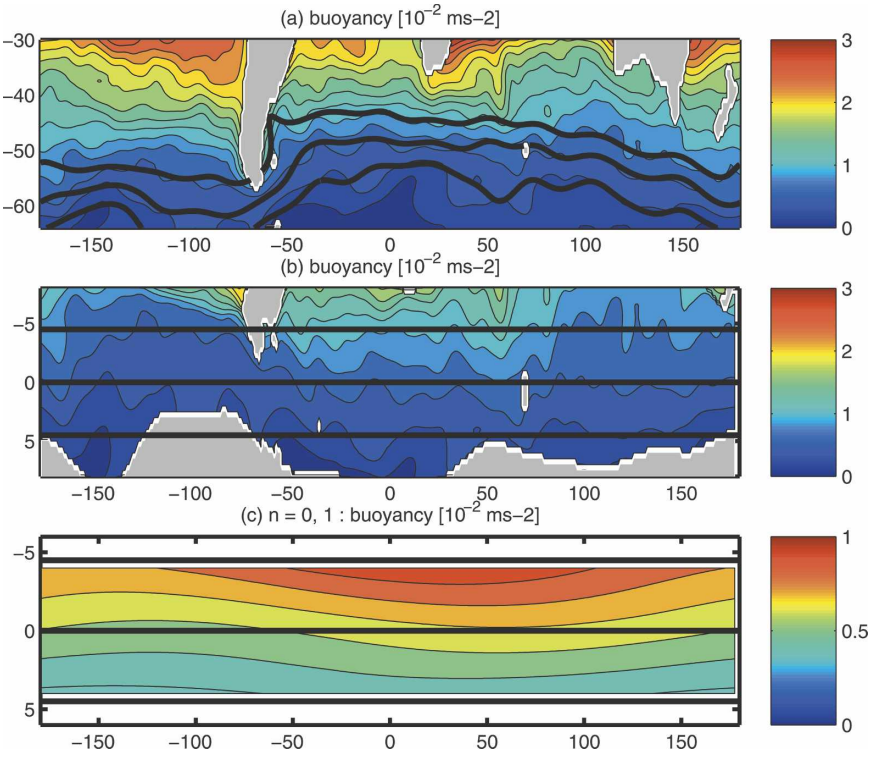

FIG. 3. The same diagnostics as in Fig. 2 is now applied to the surface buoyancy field from the Levitus climatology: (a) Mean surface buoyancy distribution in the Southern Ocean. (b) Projection of the buoyancy distribution onto the frame of reference associated with the streamfunction. (c) The filtered data consisting of the two lowest Fourier components in x.

the ACC intensify in the Atlantic–Indian sectors and weaken over the Pacific. Surface buoyancy (Fig. 3b) has a similar pattern, characterized by weak downstream variation, whereas the air–sea flux (see Fig. 4b) is highly inhomogeneous. Buoyancy flux over the ACC is mostly positive (i.e., into the ocean) but changes sign in the eastern Pacific (120°–60°W).

The following discussion will focus on the dynamics of the long-wave components, and therefore we also show (in Figs. 2c, 3c, and 4c) the filtered data for (τ, B, b_m) consisting of the two lowest Fourier components in x: the streamline-average mode and the fundamental harmonic. Fourier analysis indicates that the large-scale variation in surface buoyancy and air–sea buoyancy flux are very much in phase with each other, but shifted somewhat to the west relative to the phase of the wind stress. In addition to the Fourier analysis of the forcing fields, we have also examined the variation in the width of the ACC, defined here by the distance between $\psi_g = -5 \times 10^4\ \mathrm{m^2\ s^{-1}}$ and $\psi_g = 5 \times 10^4\ \mathrm{m^2\ s^{-1}}$ streamlines. The average width of the ACC is 11.7° latitude, whereas its first Fourier component has an amplitude of 0.6°—only 5% of the mean. Thus, the long-wave variability in the width of the ACC is much weaker than the variability in the wind stress and the air–sea fluxes, the consequences of which will be explored in the following theoretical model. Our objective is to study how these surface forcing fields drive and interact with large-scale motions in the interior of the ACC and thereby shape the three-dimensional patterns of buoyancy and meridional overturning in the Southern Ocean.

3. Formulation

a. Elements of residual-mean theory

Our starting point is the three-dimensional time-mean equations of motion. We ignore the inertial terms in the time-mean momentum equations, and write them as

$$-f\upsilon = -\frac{\partial P}{\partial x} + \frac{\partial \tau_x}{\partial z} \quad \text{and}$$
$$fu = -\frac{\partial P}{\partial y} + \frac{\partial \tau_y}{\partial z}, \tag{1}$$

where (u, υ) are the horizontal components of the Eulerian-mean velocity $\mathbf{v}$; (τ_x, τ_y) are the wind stress components, which we assume to be significant only in a

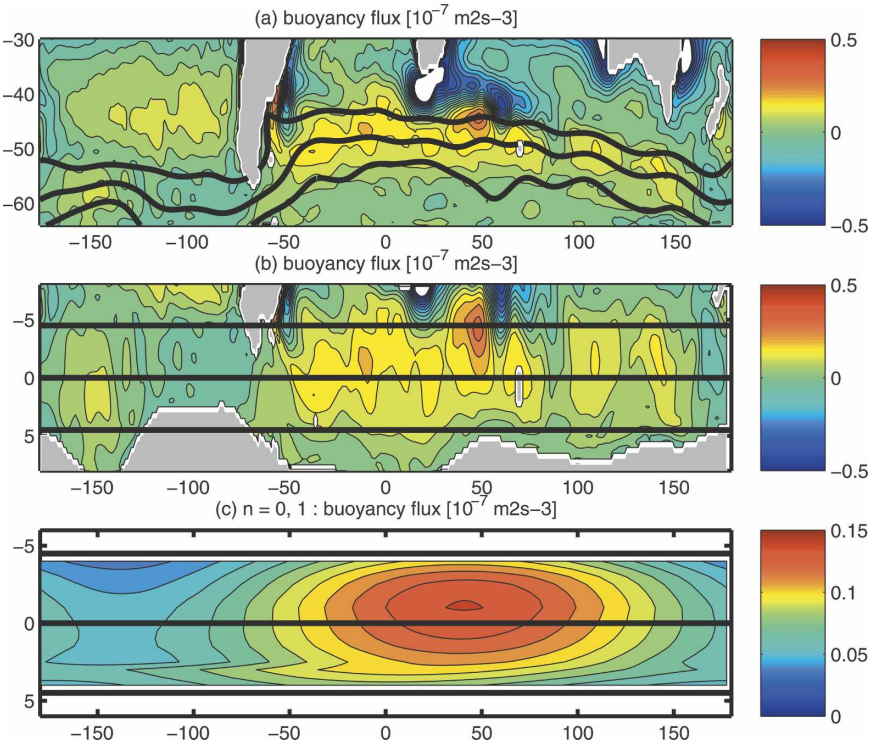

FIG. 4. The same diagnostics as in Figs. 2 and 3 but for the air–sea buoyancy flux based on the NCEP–NCAR reanalysis (positive is into the ocean).

surface boundary layer; and P is the dynamical pressure. The time-mean buoyancy equation is

$$\mathbf{v} \cdot \nabla b = -\nabla \cdot (\overline{\mathbf{v}'b'}) + \frac{\partial B}{\partial z}, \tag{2}$$

where b is the time-mean buoyancy and primes denote the perturbations from this mean due to transient eddies; B represents the vertical buoyancy flux due to small-scale processes and air–sea fluxes. In application to the ACC we interpret x as the along-stream coordinate; y is the coordinate normal to the stream, referenced to a mean surface geostrophic contour.

Andrews and McIntyre (1976) showed that it is possible to incorporate the eddy-flux terms in the Eulerian equations by introducing "residual velocities" given by

$$\mathbf{v}_{\text{res}} = \mathbf{v} + \mathbf{v}^*, \tag{3}$$

where $\mathbf{v}^* = (u^*, v^*, w^*)$ is the eddy-induced velocity of residual-mean theory, which is assumed to be nondivergent:

$$\nabla \cdot \mathbf{v}^* = \nabla \cdot \mathbf{v} = 0. \tag{4}$$

We also require that the vertical velocity (w^*) is zero at the surface ($z = 0$), and therefore integration of (4) from the surface to depth z results in

$$w^* = \frac{\partial}{\partial x}\Psi_u^* + \frac{\partial}{\partial y}\Psi_v^*,$$

where $\Psi_u^* = -\int_0^z u^*\, dz$ and $\Psi_v^* = -\int_0^z v^*\, dz$ are components of a vector streamfunction. The eddy velocities can be compactly written as follows:

$$(u^*, v^*) = -\frac{\partial}{\partial z}\Psi^* \quad \text{and}$$
$$w^* = \nabla_h \cdot \Psi^*, \tag{5}$$

where $\Psi^* = (\Psi_u^*, \Psi_v^*)$.

In appendix A we relate the vector streamfunction Ψ^* to the eddy buoyancy fluxes ($\overline{\mathbf{v}'b'}$)—see Eq. (A6). The resulting model provides a physical basis for a parameterization scheme in which the eddy streamfunction (beneath the vertically homogeneous mixed layer) is determined by the local isopycnal slope (s_x, s_y) as follows:

$$\Psi_u^* = k_0 s_x |s_x|, \quad u^* = -k_0 \frac{\partial}{\partial z}(s_x|s_x|),$$

and

$$\Psi_v^* = k_0 s_y |s_y|, \quad v^* = -k_0 \frac{\partial}{\partial z}(s_y|s_y|), \tag{6}$$

where k_0 is a constant that sets the magnitude of the eddy transfer process. This parameterization is a direct extension of a two-dimensional closure introduced in

MR and supported by the laboratory experiments in Cenedese et al. (2004).

The buoyancy equation, written in terms of the residual velocities (see appendix A), reduces to

$$\mathbf{v}_{\mathrm{res}} \cdot \nabla b = \frac{\partial \tilde{B}}{\partial z}, \tag{7}$$

where $\tilde{B} = B + B^*$ includes the explicit buoyancy forcing (B) and a contribution from residual fluxes due to diabatic eddies (B^*). In the upper ocean eddies are affected by the presence of the surface, tending to suppress the vertical component of the eddy fluxes. As a result, the eddy buoyancy transfer becomes directed across the isopycnals, which contributes to the conversion of the water masses in the mixed layer (Karsten et al. 2002). However, the estimates in MR suggest that the explicit buoyancy forcing B exceeds B^*, and therefore in the following discussion we will mostly associate $\tilde{B}$ with the direct air–sea buoyancy fluxes. The assumption that the diabatic eddy fluxes in the mixed layer play a secondary role in the dynamics of the ACC is subsequently verified (section 6).

The interior flow is assumed to be fully adiabatic; our model does not take into account either the diabatic effects of mesoscale eddies or the diapycnal mixing by small-scale turbulence below the mixed layer. Of course, both are present in the ocean; it is still a matter of debate, however, to what extent the diabatic processes affect the stratification and meridional overturning in the Southern Ocean. Numerical eddy-resolving simulations (e.g., Kuo et al. 2005) indicate that eddy transfer below the diabatic near-surface layer is directed predominantly along the isopycnal surfaces, and therefore diabatic effects of eddies at depth may not be critical for the overall structure of the ACC. Our adiabatic model can be viewed in this regard as an extreme limit, which we believe captures the essential physics of the ACC and allows for analytical treatment of the problem.

b. Quasi-zonal jet approximation

Our study is focused on a regime in which departure of the solution from its along-stream average is asymptotically small. As shown below, this approximation makes it possible to theoretically analyze three-dimensional effects, while retaining a direct connection with the two-dimensional ACC model in MR.

To develop a linear theory for the quasi-zonal current, we search for a solution by expanding in a parameter

$$\varepsilon = \frac{\langle b_1 \rangle}{\langle b_0 \rangle} \ll 1,$$

which measures the variation in buoyancy along the streamlines of the ACC relative to the cross-stream variation. Inspection of the surface buoyancy field in Fig. 3c indicates that $\varepsilon \sim 0.1$, which justifies the asymptotic expansion in ε. Next, we separate the mean variables into the dominant two-dimensional part [a function of (y, z) only] and a weak ($\sim\varepsilon$) three-dimensional component. The linear analysis is focused on the dynamics of the fundamental harmonic in x:

$$\begin{aligned}
\mathbf{v} &= \mathbf{v}_0(y, z) + \mathbf{v}_1(x, y, z) + \cdots, \quad \mathbf{v}_1 = \mathrm{Re}[\hat{\mathbf{v}}_1(y, z)\exp(ikx)],\\
\mathbf{v}^* &= \mathbf{v}_0^*(y, z) + \mathbf{v}_1^*(x, y, z) + \cdots, \quad \mathbf{v}_1^* = \mathrm{Re}[\hat{\mathbf{v}}_1^*(y, z)\exp(ikx)], \quad \text{and}\\
b &= b_0(y, z) + b_1(x, y, z) + \cdots, \quad b_1 = \mathrm{Re}[\hat{b}_1(y, z)\exp(ikx)],
\end{aligned} \tag{8}$$

where k is a wavenumber. The subscripts (0, 1) in (8) pertain to (zero, first)-order quantities in ε. We also isolate the streamline average and the fundamental harmonic of the surface forcing fields—wind stress and the air–sea buoyancy flux (although no assumption is made as to the relative amplitudes of their spectral components):

$$\begin{aligned}
B &= B_0(y, z) + B_1(x, y, z) + \cdots, \quad B_1 = \mathrm{Re}[\hat{B}_1(y, z)\exp(ikx)], \quad \text{and}\\
\tau_x &= \tau_{0x}(y) + \tau_{1x}(x, y) + \cdots, \quad \tau_1 = \mathrm{Re}[\hat{\tau}_{1x}(y)\exp(ikx)],
\end{aligned}$$

where B is the buoyancy forcing in (7) and τ_x is the zonal component of the wind stress.

To illustrate the expansion procedure, we write the buoyancy equation in (7) as follows:

$$(\mathbf{v}_0 + \mathbf{v}_1 + \cdots) \cdot \nabla(b_0 + b_1 + \cdots) + (\mathbf{v}_0^* + \mathbf{v}_1^* + \cdots) \cdot \nabla(b_0 + b_1 + \cdots) = \frac{\partial B_0}{\partial z} + \frac{\partial B_1}{\partial z} + \cdots.$$

The leading (zero order) balance in ε is

$$\mathbf{v}_{0\,\mathrm{res}} \cdot \nabla b_0 = \frac{\partial B_0}{\partial z}, \tag{9}$$

whereas the first-order balance for the fundamental harmonic in x requires that

$$\mathbf{v}_{1\,\mathrm{res}} \cdot \nabla b_0 + \mathbf{v}_{0\,\mathrm{res}} \cdot \nabla b_1 = \frac{\partial B_1}{\partial z}. \tag{10}$$

The momentum equations in (1), continuity equation in (4), and the eddy closure in (6) are similarly expanded in powers of ε. Not surprisingly, at zero order in ε we recover a set of equations identical to those used in the two-dimensional model (MR), which is briefly reviewed below. The first-order correction, on the other hand, will give us information about longitudinal variations in the stream, the information that we seek.

c. Zero-order solution: The ACC in two dimensions

The zero-order component of the (y, z) velocities can be expressed in terms of the scalar streamfunctions (time mean and eddy induced) as follows:

$$\upsilon_0^* = -\frac{\partial \Psi_0^*}{\partial z}, \qquad w_0^* = \frac{\partial \Psi_0^*}{\partial y},$$
$$\upsilon_0 = -\frac{\partial \Psi_0}{\partial z}, \quad \text{and} \quad w_0 = \frac{\partial \Psi_0}{\partial y},$$

and the residual circulation is described by the streamfunction $\Psi_{0\,\mathrm{res}}(y, z) = \Psi_0 + \Psi_0^*$.

The eddy parameterization (6) at leading order reduces to

$$\Psi_0^* = k_0 |s_0| s_0 = -k_0 s_0^2,$$
$$\upsilon_0^* = -\frac{\partial \Psi_0^*}{\partial z} = k_0 \frac{\partial}{\partial z} s_0^2, \quad \text{and} \quad s_0 = -\frac{b_{0y}}{b_{0z}}, \tag{11}$$

and the zero-order y-momentum equation is

$$-f\upsilon_0 = \frac{\partial \tau_0}{\partial z}. \tag{12}$$

The problem is solved separately in a thin, vertically homogeneous mixed layer ($-h_m < z < 0$) and in the stratified interior ($z < -h_m$). For the interior it is assumed that eddies are adiabatic, and the forcing, mechanical and thermodynamical (B, τ), vanishes. Hence, the buoyancy equation (9) reduces to

$$J(\Psi_{0\,\mathrm{res}}, b) = 0, \tag{13}$$

where $J(A, B) \equiv A_y B_z - A_z B_y$. Equation (13) implies that the residual streamfunction and buoyancy are functionally related: $\Psi_{0\,\mathrm{res}} = \Psi_{0\,\mathrm{res}}(b_0)$.

Integrating the buoyancy equation in (2) over the depth of the vertically homogeneous mixed layer ($-h_m < z < 0$), for the (two dimensional) zero-order component we obtain

$$\Psi_{0\,\mathrm{res}|z=-h_m} \frac{\partial b_{0m}}{\partial y} = B_0, \tag{14}$$

where b_{0m} is the surface buoyancy. Integrating the momentum equation in (12) vertically from the surface to depth z (noting that $\Psi_0 = 0$ at the surface and τ is zero at depth), we find that $f\Psi_0 = -\tau_0$. Because $\Psi_{0\,\mathrm{res}}(y, z) = \Psi_0 + \Psi_0^*$, we arrive at, using (11), the key relationship of the MR model:

$$\Psi_{0\,\mathrm{res}}(b_0) = -\left(\frac{\tau_0}{f} + k_0 s_0^2\right). \tag{15}$$

This equation can be easily integrated (see MR) along isopycnal surfaces: an algebraic transformation shows that the isopycnals represent the characteristics of (15), and the characteristic velocities υ_c and w_c are

$$\frac{dy}{dl} = \upsilon_c = 1 \quad \text{and}$$
$$\frac{dz}{dl} = w_c = s_0 = -\frac{b_{0y}}{b_{0z}} = -\sqrt{-\frac{\tau_0}{fk_0} - \frac{\Psi_{0\,\mathrm{res}}}{k_0}}. \tag{16}$$

Of course, $\Psi_{0\,\mathrm{res}}$ and b_0 do not change at a point moving along the characteristics, and therefore, for any given distribution of surface buoyancy and air–sea fluxes, the interior solution can be obtained by integrating the characteristic equations in (16) downward from the surface. If, however, the surface $\Psi_{0\,\mathrm{res}}$ or b_0 are unknown, as in the problem solved in section 5, the method of characteristics can be readily modified to include an iterative adjustment to specified surface and boundary conditions.

d. First-order correction

To proceed to the next order, we rewrite the first-order buoyancy budget (10) in terms of the complex amplitudes of the fundamental harmonics of residual velocity and buoyancy ($\hat{\mathbf{v}}_{1\,\mathrm{res}}, \hat{\mathbf{b}}_1$). Since the x component of the eddy-induced velocity does not appear at this order—the parameterization in (6) implies that $u^* = O(\varepsilon^2)$—(10) reduces to

$$\hat{\upsilon}_{1\,\mathrm{res}} \frac{\partial b_0}{\partial y} + \hat{w}_{1\,\mathrm{res}} \frac{\partial b_0}{\partial z} + u_0 ik \hat{b}_1 + \upsilon_{0\,\mathrm{res}} \frac{\partial \hat{b}_1}{\partial y} + w_{0\,\mathrm{res}} \frac{\partial \hat{b}_1}{\partial z} = \frac{\partial \hat{B}_1}{\partial z}. \tag{17}$$

The continuity equation (4) at $O(\varepsilon)$ is

$$ik\hat{u}_1 + \frac{\partial \hat{v}_{1\,\mathrm{res}}}{\partial y} + \frac{\partial \hat{w}_{1\,\mathrm{res}}}{\partial z} = 0. \tag{18}$$

To simplify the algebra, it is also convenient to introduce the following $O(\varepsilon)$ variables:

$$\psi_1^* \equiv -\int_0^z \hat{v}_1^*\, dz \quad \text{and}$$
$$\psi_{1\,\mathrm{res}} \equiv -\int_0^z \hat{v}_{1\,\mathrm{res}}\, dz, \tag{19}$$

which represent the first-order terms in the ε expansion of the eddy streamfunction Ψ_v^* in (6) and the corresponding residual streamfunction. The integral of the continuity equation (18) in z yields, after applying boundary conditions,

$$\hat{w}_{1\,\mathrm{res}} = \frac{\partial \psi_{1\,\mathrm{res}}}{\partial y} - ik\int_0^z \hat{u}_1\, dz. \tag{20}$$

Solution of the perturbation equations in (17)–(20) is greatly simplified by introducing a coordinate system associated with the zero-order buoyancy surfaces. As shown in appendix B, an algebraic transformation reduces the system of partial differential equations in (y, z) in (17)–(20) to a system of *ordinary* differential equations in variable l, which measures the distance along the "old" zero-order isopycnals:

$$\frac{d\hat{b}_1}{dl} - \frac{(\psi_{1\,\mathrm{res}} + \hat{\tau}_{1x}/f)b_{0z}}{2k_0 s_0} = ik\frac{b_{0z}\displaystyle\int_0^z \hat{P}_1\, dz}{2k_0 s_0 f} \quad \text{and}$$
$$\frac{d\psi_{1\,\mathrm{res}}}{dl} - \left(\frac{d\Psi_{0\,\mathrm{res}}}{db_0}\right)\frac{d\hat{b}_1}{dl} + ik\frac{u_0\hat{b}_1}{b_{0z}} = ik\int_0^z \hat{u}_1\, dz, \tag{21}$$

where d/dl is defined in (16). Dynamical pressure and the zonal velocity in (21) are related to the buoyancy by the hydrostatic and geostrophic relations:

$$\hat{P}_1 = \int_{-h}^z \hat{b}_1\, dz \quad \text{and} \quad \hat{u}_1 = -\frac{1}{f}\frac{\partial \hat{P}_1}{\partial y}, \tag{22}$$

where h is the depth of the model thermocline.

In what follows, we solve the linearized problem by integrating the system of coupled ordinary differential equations for ($\hat{b}_1$, $\psi_{1\,\mathrm{res}}$) in (21) downward from the base of the mixed layer into the interior along the zero-order isopycnals. Essentially, the method of characteristics, introduced in section 3c for the two-dimensional problem, is extended to three dimensions. Implementation of this method depends on a particular choice of surface and boundary conditions, and specific details are given in sections 4 and 5. However, in every case integration of (21) requires knowledge of $\psi_{1\,\mathrm{res}}$ at the base of the mixed layer. In appendix B, we derive the (order ε) perturbation equations for the mixed layer and show that $\psi_{1\,\mathrm{res}}$ can be expressed as

$$\psi_{1\,\mathrm{res}}(-h_m) = \frac{\hat{B}_1 - \Psi_{0\,\mathrm{res}}(-h_m)\dfrac{\partial}{\partial y}\hat{b}_{1m} - iku_0\hat{b}_{1m}h_m}{\dfrac{\partial}{\partial y}b_{0m}}. \tag{23}$$

Equations (21) and (23) are the key elements of our model that, as we now show, makes it possible to readily obtain steady linear three-dimensional solutions for the ACC and its overturning circulation.

4. Diagnostic model: Prescribing the surface buoyancy and the air–sea fluxes

The simplest problem that can be treated by the method of characteristics, and the one that was solved in two dimensions by MR, involves prescribing the surface buoyancy distribution (b_m), wind stress (τ_x), net buoyancy forcing (B), and computing the resulting interior distribution of buoyancy and residual circulation. To relate our theoretical results to the observations, it is convenient to set the origin of the coordinate system at 180°. This projects the longitude range from −180 eastward to 180° in Figs. 2, 3, and 4 onto the computational interval $0 < x < L_x = 2\pi/k$ in our model; the zero longitude therefore corresponds to $x = 0.5L_x$. The two lowest spectral components of (τ_x, b_m, B) in Figs. 2c, 3c, and 4c are closely approximated by the following analytical expressions for wind stress:

$$\tau_x = \tau_{0x}(y) + \mathrm{Re}[\hat{\tau}_{1x}(y)\exp(ikx)],$$
$$\tau_{0x} = \tau_{00}\left[0.6 + \sin\left(\pi\frac{y}{L_y}\right)\right],\ \tau_{00} = 0.0001\ \mathrm{m^2\,s^{-2}},\quad \text{and}$$
$$\hat{\tau}_{1x} = 0.3\exp(0.5\pi i)\tau_{0x}; \tag{24}$$

for buoyancy:

$$b_m = b_{0m} + \mathrm{Re}(\hat{b}_{1m}\exp(ikx)],$$
$$b_{0m} = (y/L_y)\Delta b,\ \Delta b = 0.015\ \mathrm{m\,s^{-2}},\quad \text{and}$$
$$\hat{b}_{1m} = -0.07\exp(-0.3\pi i)\Delta b\sin\left(\pi\frac{y}{L_y}\right); \tag{25}$$

and for air–sea flux:

$$B = B_0 + \mathrm{Re}[\hat{B}_1 \exp(ikx)],$$
$$B_0 = B_{00} \sin\left(\pi \frac{y}{L_y}\right), B_{00} = 7 \times 10^{-9}\ \mathrm{m^2\ s^{-3}}, \quad \text{and}$$
$$\hat{B}_1 = -0.5(1 - i)B_0. \tag{26}$$

Two technical issues should be mentioned with regard to the projection of the data onto our along/cross-stream (x, y) coordinate system. First, we work in Cartesian coordinates and do not attempt to represent details of spherical geometry. Second, our regridding technique does not take into account variation in the width of the circumpolar current. This approximation is based on the Fourier analysis of observations (see section 2), which shows that the fundamental harmonic of the ACC width is only 5% of its mean value—much less that the relative amplitude of the fundamental harmonic of the air–sea flux (100% of the mean) or the variation in the wind stress (20% of the mean). While this approximation introduces a minor error in the momentum and buoyancy budgets, its effect is considerably weaker than the uncertainty in the magnitudes of the forcing fields in observations.

The mixed layer depth is set at $h_m = 100$ m, and the constant that sets the magnitude of the eddy transfer coefficients K (see the appendix A) is $k_0 = 10^6\ \mathrm{m^2\ s^{-1}}$, as estimated and used in MR. The zonal extent of the channel is $L_x = 20\,000$ km, and the width of the model current is $L_y = 2000$ km. As discussed earlier (sections 1 and 2), the patterns of buoyancy and buoyancy flux anomalies represent the enhanced warming of the ACC in the Atlantic and Indian Ocean regions and cooling east of Australia (see Fig. 4). The complex coefficients in the $\hat{b}_1$, $\hat{\tau}_{1x}$, and $\hat{B}_1$ terms reflect the phase of the fundamental (in x) harmonic relative to the $-180°$ to $180°$ interval.

The zero-order interior fields of buoyancy and residual circulation are obtained by integrating Eqs. (16) as in MR. The resulting solution, for surface conditions in (24)–(26), is shown in Fig. 5. The depth of the model thermocline reaches 2 km on the equatorward flank of the ACC, not unlike the observations discussed in Karsten and Marshall (2002a). The sense of the residual circulation corresponds to upwelling of fluid in the deep layers that outcrop at the poleward flank of the ACC; fluid is subducted downward and equatorward in the upper layers. The net strength of the overturning circulation is 18 Sv (Sv $\equiv 10^6\ \mathrm{m^{-3}\ s^{-1}}$), which is comparable to the earlier observational estimates (e.g., Karsten and Marshall 2002b) and the zonal-average theoretical model of MR.

The next step is to compute the $O(\varepsilon)$ quantities. For

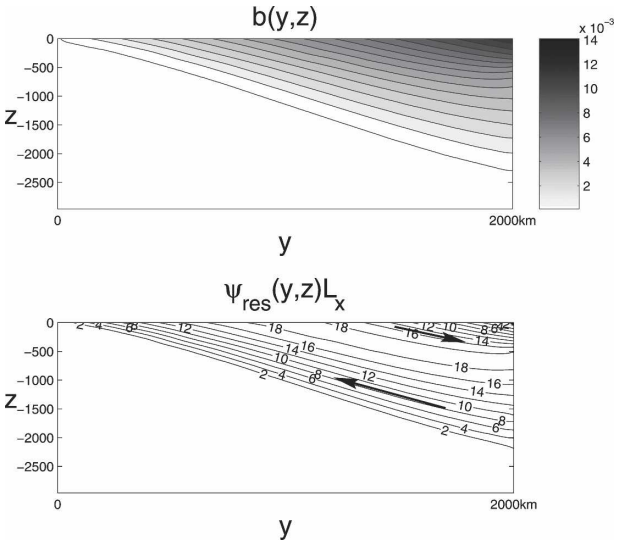

FIG. 5. The (top) buoyancy (m s^{-2}) and (bottom) residual circulation for the zero-order (2D) component, multiplied by L_x to represent the net strength of the overturning circulation (Sv).

a prescribed buoyancy distribution in the mixed layer ($\hat{b}_{1m}$), $\psi_{1\ \mathrm{res}}(-h_m)$ is obtained from Eq. (23). Knowing ($\psi_{1\ \mathrm{res}}$, $\hat{b}_1$) at the bottom of the mixed layer, we integrate the interior equations in (21) along the zero-order (hence already known) characteristics. This integration, however, requires knowledge of the terms on the right-hand side of (21), which, in our case, have to be obtained as a part of the solution. These terms are computed using an iterative procedure. First we solve (21) ignoring the rhs terms, and then use the resulting solution to evaluate them; pressure and zonal velocity are obtained from (22). The integration along the characteristics is repeated consecutively, and on each iteration we use the estimate of the rhs terms from the previous step. Typically, it takes less than 10 such iterations for the model to converge, within a negligible error of $\sim 10^{-8}$, to a sought-after solution.

The total buoyancy and velocity fields are obtained by adding the two-dimensional zero-order components and the $O(\varepsilon)$ correction (8). Figure 6a shows the distribution of w_{res} at $z = -h_m$; this quantity indicates the location and strength of the flux of buoyancy and passive tracers into (from) the diabatic mixed layer. The overturning circulation, as measured by w_{res}, is characterized by a strong—comparable to the mean—downstream variation.[2] The amplitude of w_{res} is relatively

[2] Recall that our linear theory makes no assumptions as to the relative strength of the zonally averaged and 3D components of the *residual* circulation.

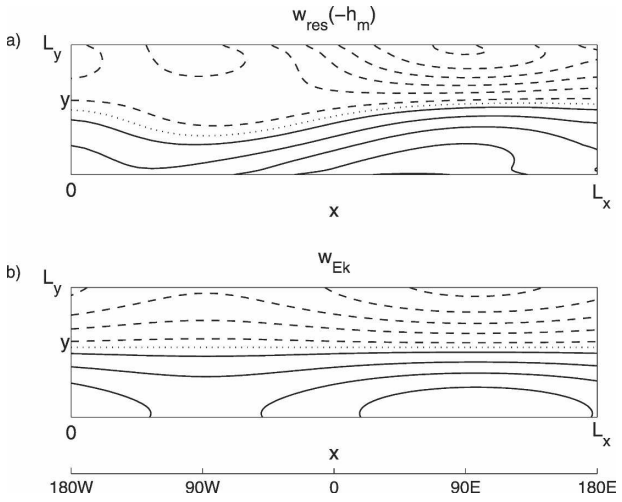

FIG. 6. (a) The vertical component of the residual velocity at the bottom of the mixed layer. The strength of the overturning circulation, as measured by $w_{\rm res}$ increases in the eastern part of the domain (Atlantic–Indian sectors) and decreases in the Pacific region ($x < L_x/3$). (b) Ekman velocity. Note the significant difference between $w_{\rm res}$ and $w_{\rm Ek}$. Positive (negative) contours start at 0.25×10^{-6} m s^{-1} (-0.25×10^{-6} m s^{-1}) and are indicated by solid (dashed) curves. The contour interval is 0.5×10^{-6} m s^{-1}, and the zero contours are represented by the dotted line. Note that 10^{-6} m s^{-1} $\approx$ 30 m yr^{-1}.

weak for $0 < x < L_x/3$ (an interval corresponding to 180°–60°W) but greatly intensifies after $x = L_x/3$, reaching values of 2×10^{-6} m s^{-1} $\approx$ 60 m yr^{-1}. Thus, our model predicts that the meridional overturning cell (MOC) in the Southern Ocean is greatly reduced in strength in the Pacific sector, but enhanced in the Atlantic–Indian sector. Note the considerable difference in the structure and amplitude of $w_{\rm res}$ in Fig. 6a and the Ekman pumping in Fig. 6b, which indicates the significance of eddy advection for the overturning circulation in the Southern Ocean.

5. Solving for the surface buoyancy and buoyancy flux

While the foregoing setup is internally consistent and provides an important diagnostic tool for the dynamics of the ACC, one can readily question some of the implicit assumptions in the formulation of the model. In particular, the surface buoyancy distribution and/or the air–sea fluxes, which have been prescribed in section 4, in reality may be a consequence of internal dynamics of the ACC and its interaction with the adjacent subtropical gyres. Although the issue of causality is beyond the scope of the present study, we now consider alternative, and perhaps more physically motivated, upper boundary conditions.

In the following example we suppose that the surface buoyancy distribution and the air–sea fluxes are not known and should be computed as a part of the problem. Instead, the mixed layer buoyancy $b_m(x, y)$ is relaxed to a target buoyancy distribution $b^* \approx b^*(y) + \mathrm{Re}[\hat{b}_1^*(y) \exp(ikx)]$, which, we assume, is set by the atmosphere and therefore is to be regarded as known. The surface buoyancy flux is parameterized accordingly:

$$B = -\lambda(b_m - b^*). \tag{27}$$

In this calculation we use $\lambda = 9 \times 10^{-6}$ m s^{-1}, which, for $h_m \sim$100 m, corresponds to a relaxation time scale of about 2 months; the resulting solutions show little sensitivity to the specific value chosen for this parameter.

Inspection of the near-surface atmospheric temperature (not shown) suggests that b^* can be approximated by the following simple analytical function:

$$\begin{aligned} b^* &= b_0^* + \mathrm{Re}[\hat{b}_1^* \exp(ikx)], \\ b_0^* &= (y/L_y)\Delta b, \ \Delta b = 0.015 \text{ m s}^{-2}, \quad \text{and} \\ \hat{b}_1^* &= -0.1 \exp(-0.3\pi i)\Delta b \sin\left(\pi \frac{y}{L_y}\right), \end{aligned} \tag{28}$$

which only slightly differs from the surface buoyancy distribution (25) used in our previous model (section 4). We emphasize that the longitudinal variation in b^* in our theory should be interpreted as a result of the meridional displacement of the ACC in physical coordinates. As the ACC circumnavigates the globe, it shifts toward the warm lower latitudes in the Atlantic–Indian sectors and returns poleward as it passes through the Pacific sector. Thus, when the atmospheric temperature is projected onto the streamline coordinate system, it acquires a distinct signal in the fundamental Fourier component in x, the signal which may be absent in the original (latitude–longitude) frame of reference.

At the same time, it is sensible to consider the vertical distribution of buoyancy on the equatorial flank of the ACC as given. If the ACC ($y < L_y$) merges continuously with a subtropical gyre on the equatorial flank ($y > L_y$), then the stratification at $y = L_y$ may be affected, or even determined, by the dynamics of the subtropical thermocline. According to Karsten and Marshall (2002a), the stratification on the equatorial flank of the ACC can be represented by a decaying exponential with an e-folding depth of $h_e \approx 1000$ m. We therefore use

$$b|_{y=L_y} = b_N(z) = A_1 \exp(z/h_e) + A_2. \tag{29}$$

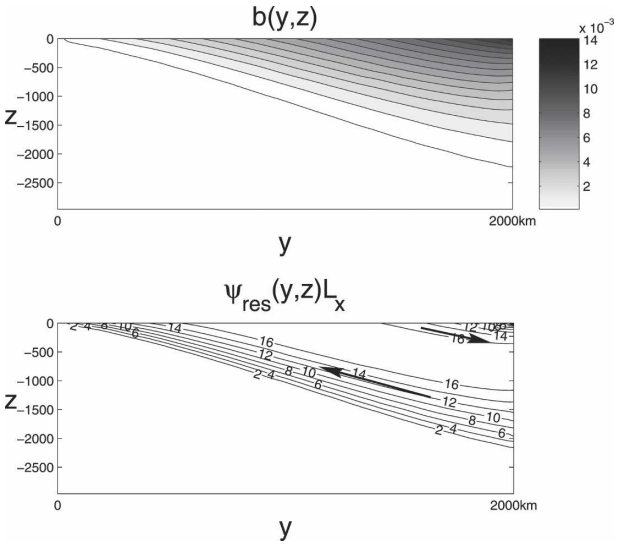

FIG. 7. The (top) streamline-averaged buoyancy (m s^{-2}) and (bottom) residual circulation for a model in which we prescribe the stratification at the northern flank of the ACC, and relax the surface buoyancy to a target distribution b^*. The residual streamfunction is multiplied by L_x to represent the net strength of the overturning circulation (Sv).

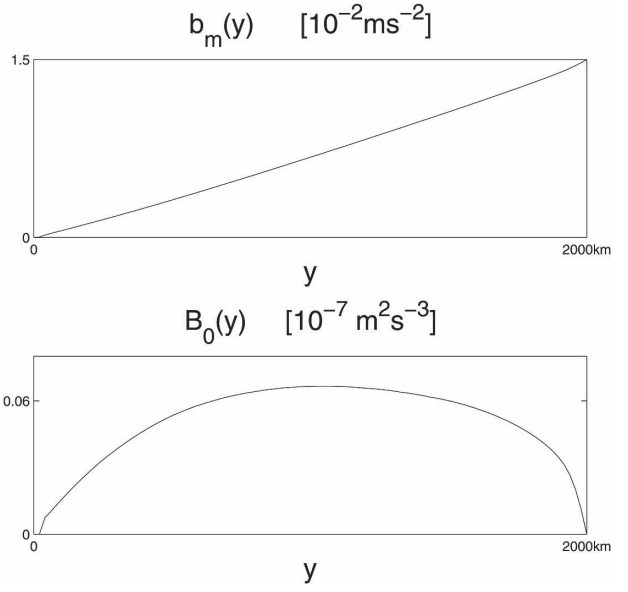

FIG. 8. The (top) streamline-averaged surface buoyancy and (bottom) air–sea buoyancy flux for the model in Fig. 7.

The constants A_1 and A_2 are determined by requiring $b_N(z = -h_m) = \Delta b$ and $b_N(z = -h) = 0$, where h is the depth of the model thermocline at $y = L_y$.

Prescribing the density distribution at $y = L_y$ requires modification of the foregoing method of characteristics; we implement the following iterative procedure. First we compute the two-dimensional zero-order solution. An initial guess is made for the surface buoyancy [we start with a linear $b_{0m}(y)$], the surface buoyancy flux is computed from (27), and the model is integrated using the method of characteristics in (16). The resulting buoyancy distribution at $y = L_y$ is compared with our target buoyancy distribution (29), and the difference between the two is used to adjust the surface buoyancy at the origin of each characteristic. The procedure is repeated until the buoyancy at $y = L_y$ converges, within an acceptable error ($\sim 10^{-8}$), to the target distribution at the northern flank (29).

The zero-order (two dimensional) components of buoyancy and residual circulation are shown in Fig. 7; this solution is similar to the one obtained with the model in section 4 (see Fig. 5). In our case, however, the model is interactive and does not rely on the a priori knowledge of the air–sea fluxes. The implied streamline-averaged buoyancy flux and surface buoyancy in the model are shown in Fig. 8. Buoyancy flux is positive (into the ocean) with a maximum amplitude of 6×10^{-9} m^2 s^{-3}, broadly consistent with the observations in Fig. 4c.

Next, the same iterative technique is applied to the three-dimensional component of circulation. Equations (21) are consecutively integrated along the zero-order characteristics; on each iteration the value of surface buoyancy at the origin of each characteristic (b_{1m}) is adjusted to reduce the amplitude of b_1 at the point where this characteristic crosses the northern boundary ($y = L_y$). The procedure is repeated until b_1 converges to zero at the equatorward flank of the ACC: $b_{1|y=L_y} = 0$. The resulting distribution of buoyancy for surface and boundary conditions prescribed in (27)–(29) is shown in Fig. 9. The zonal buoyancy section along the center ($y = 0.5L_y$) of the model current is characterized by a pronounced warming, increase in stratification and upper-thermocline depth in the eastern region $0.5L_x < x < L_x$ (0°–180°). These model predictions are consis-

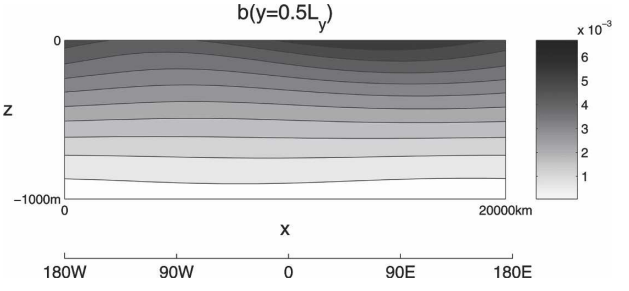

FIG. 9. Zonal buoyancy (m s^{-2}) cross section of the model ACC along $y = 0.5L_y$. Note the warming, increase in stratification, and the upper thermocline depth in the eastern part of the section.

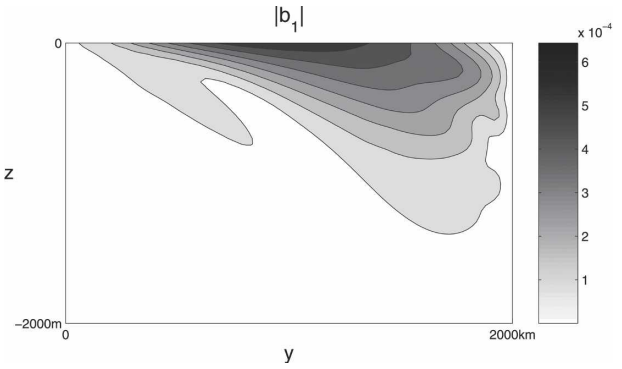

FIG. 10. The absolute value of the complex amplitude of the fundamental harmonic of buoyancy (m s^{-2}) is plotted as a function of y and z; $|b_1|$ indicates the magnitude of the buoyancy variation along the streamfunction contours of the ACC. Comparison with the streamline average in Fig. 7 (top panel) indicates that the downstream variability is generally weak relative to the mean (~5%).

tent with oceanographic observations; see, for example, the recent data analysis by Sun and Watts (2002). These authors present streamfunction projections of the historical hydrographic data, the frame of reference directly associated with our (x, y) coordinates, and the pattern of buoyancy in Fig. 9 is suggestive of the observed temperature field along the streamline in Fig. 11 of Sun and Watts (2002).

Figure 10 reveals the spatial pattern of the downstream variation in buoyancy. The amplitude of b_1—the fundamental harmonic in x—is plotted as a function of y and z. Figure 10 indicates that most of the downstream variability in the model occurs in the upper ocean (at depths ~500 m or less) on the equatorward side of the ACC. This feature also finds support in observations (see, e.g., Fig. 9 in Sun and Watts 2002). The maximum downstream buoyancy variation in our model occurs at the surface and its amplitude is $\sim 7 \times 10^{-4}$ m s^{-2}, which corresponds to the temperature variation ~1°C. It should be emphasized, however, that the variability shown in Fig. 10 represents only the contribution from the first longitudinal spectral mode and does not include high-wavenumber components.

The implied patterns of the surface buoyancy and the air–sea flux are shown in Fig. 11. While the downstream buoyancy variation is very gentle, less than 10% of the cross-stream buoyancy difference, the air–sea flux in Fig. 11a is highly nonuniform. The amplitudes of the zero and first spectral harmonics are comparable, leading to their approximate cancellation in the eastern Pacific Ocean and intensification in the Atlantic–Indian sector ($L_x/3 < x < 2L_x/3$ in the model). Compelling evidence in support of the theory comes from comparing our solutions with the corresponding low modes of the observed air–sea flux and buoyancy in Figs. 3c and 4c. Both phase and amplitude of the observed buoyancy and the air–sea flux are captured by the model predictions in Figs. 11a and 11b.

Last, it is of interest to examine the distribution of

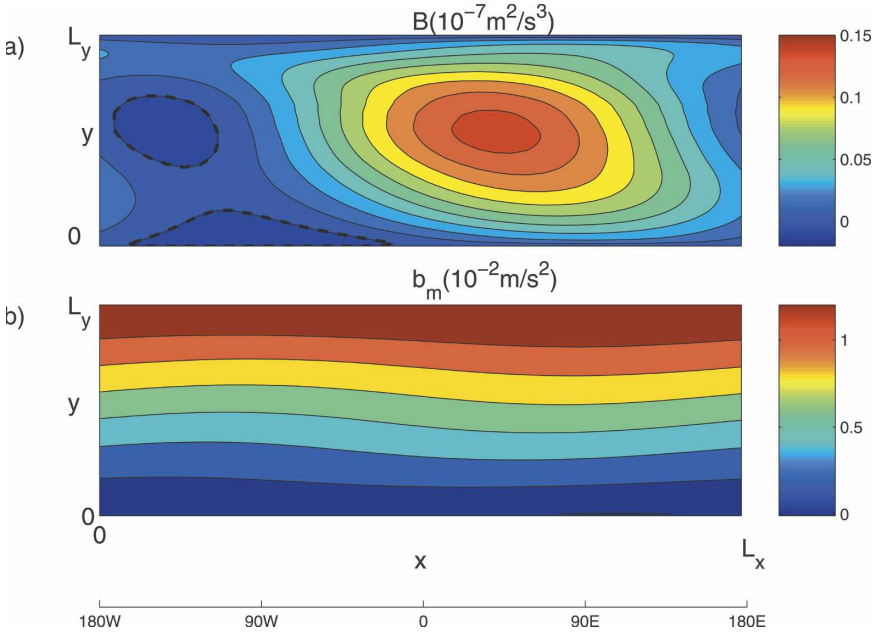

FIG. 11. (a) Implied air–sea buoyancy flux in the model (zero contour is marked by the dashed line). (b) The mixed layer buoyancy.

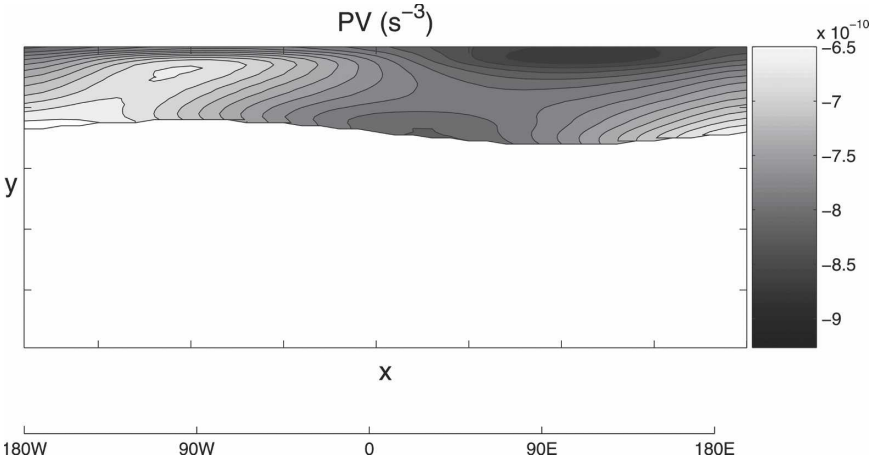

FIG. 12. Distribution of the potential vorticity PV = $f\partial b/\partial z$ on the isopycnal surface with $b = (2/3)\Delta b$. Note the region of low-PV fluid in the upper-left corner of the plot (counterpart of the southeastern Pacific).

the large-scale potential vorticity PV = fb_z along the isopycnal surfaces in our model. In addition to being a useful dynamical tracer, the isentropic PV gradients measure the direction and strength of the residual circulation (see the discussion in MR). Figure 12 shows the distribution of the isentropic potential vorticity on the isopycnal with $b = (2/3)\Delta b$ This surface is located on the equatorward flank of the ACC in the region where the residual circulation (see Fig. 6) is directed downward from the mixed layer. An intriguing feature of the PV pattern in Fig. 12 is related to a region of low PV in the western part of the domain ($x < 0.25L_x$)—the counterpart of southeastern Pacific. This low-PV fluid apparently originates near the surface in the region of surface cooling (see Fig. 11a) and then spreads, along the isopycnal surface, downward and eastward into the main thermocline. It is tempting to relate this low-PV fluid with the Subantarctic Mode Water. Of course, mode waters are known to form convectively within the deep winter mixed layers, physics that is beyond the scope of our idealized linear model. However, our theory predicts the conditions—surface cooling and subduction—that favor the formation of the low-PV water, and thus can be used to explain its spatial distribution.

6. Physical interpretation of the model results

Inspection of the PV distribution along the buoyancy surfaces (e.g., Fig. 12) and the general structure of the solution in section 5 suggests the following interpretation of the mechanisms controlling the residual circulation of the ACC. As the ACC moves through the Pacific sector (180°–90°W), passing through the cold southern polar regions, its isentropic potential vorticity gradients are relatively weak (see Fig. 12b), which may be related to the PV homogenization[3] (e.g., Rhines and Young 1982). The absence of strong large-scale isentropic PV gradients in the Pacific in our model leads to a reduced downgradient flux of potential vorticity (and other tracers) along the buoyancy surfaces. As discussed in MR, weak isentropic eddy transfer is, in turn, directly related to a decrease in the strength of the residual circulation, which is indeed reproduced by our model (Fig. 6a).

However, as the ACC shifts equatorward east of Drake Passage, the surface temperature along its axes rises, which is revealed most clearly by the projection of the surface buoyancy onto streamlines in Fig. 3c. This feature is also reflected in the schematic diagram in Fig. 13a, which illustrates the spatial distribution of buoyancy in the frame of reference associated with the ACC. The downstream increase in buoyancy in the Atlantic–Indian sector (60°W–100°E) in Fig. 3c is accompanied by the corresponding strengthening of the meridional surface buoyancy gradient south of the $\Psi = 0$ streamline. The resulting pattern of buoyancy in the meridional plane is indicated in Fig. 13b. Since the stratification at the equatorward flank of the ACC [$b_N(z)$] does not significantly vary in y (Karsten and Marshall 2002a), an increase of the surface buoyancy

[3] Of course, the eddy parameterization used in our model (appendix A) provides a mechanism for isopycnal diffusion of thickness rather than PV. However, given the relatively limited meridional extent of the ACC (small Δf) and a significant depth variation within it (large Δh), the isentropic mixing of PV and thickness become largely equivalent.

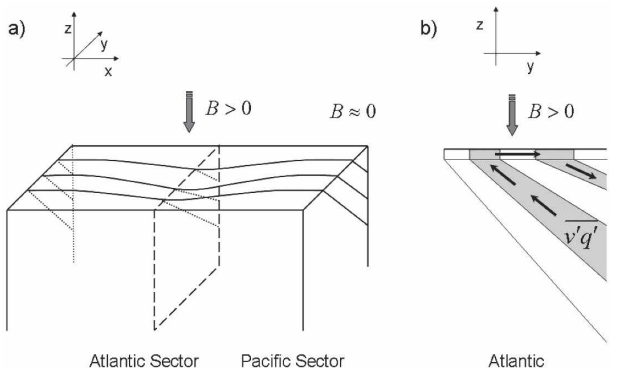

FIG. 13. Schematic diagram for the pattern of buoyancy in the ACC. (a) Three-dimensional structure of the buoyancy field. The surface buoyancy flux into the ocean in the Atlantic sector results in the poleward shift of the surface buoyancy contours relative to the stream (see the observations in Fig. 3c). (b) Distribution of buoyancy in the meridional cross section of the ACC in the Atlantic sector marked by the dashed lines in (a). Poleward shift of the surface buoyancy contours results in the interior isopycnal potential vorticity gradients. These gradients cause the downgradient PV fluxes and ultimately result in a considerable meridional overturning by the residual flow indicated by the solid arrows.

gradient on the poleward flank of the ACC in the Atlantic sector (Fig. 3c) leads to considerable isopycnal PV gradients. As indicated in Fig. 13b, PV gradients become positive immediately above the base of the ACC thermocline (isopycnal layers are thin near the surface and thicken as their depth increases toward the equator). The isopycnal PV gradients, however, change sign in the buoyant upper isopycnal layers. This pattern implies the poleward downgradient flux of PV (and thus of other tracers as well) at depth and the equatorward eddy transfer in the upper layers (see Fig. 13b), which is consistent with the structure of residual circulation predicted by the model (section 5).

a. Two-dimensional effects in the dynamics of the ACC

The foregoing model indicates that the overturning circulation greatly intensifies in the Atlantic–Indian sector, similar to the patterns of both the wind stress (τ) and air–sea flux (B), creating an impression that the response of the ACC to the external forcing may have a largely local character. Thus, we now attempt to determine whether the ACC can be viewed as a quasi-two-dimensional flow whose structure, at any given meridional cross section, is controlled by local processes. To quantify the role of the fundamentally three-dimensional effects in setting the meridional distribution of buoyancy and residual circulation—effects that result from the zonal convergence of the buoyancy and volume fluxes—we go on to diagnose the dominant balances of the residual buoyancy equation for the solution in section 5. We separately consider the upper mixed layer and stratified interior.

The first-order ($\sim\varepsilon$) component of the buoyancy equation in the mixed layer is given by (B12) in appendix B, and the partitioning of terms in the buoyancy budget is shown in Fig. 14. The upper plots present, for each y, the amplitude (Fig. 14a) and phase (Fig. 14b) of the zonal advection term

$$T_u(y) = iku_0\hat{b}_{1m}h_m, \tag{30}$$

whereas the term resulting from the meridional advection of buoyancy by the residual flow

$$T_v(y) = \psi_{1\,\mathrm{res}}\frac{\partial b_{0m}}{\partial y} + \Psi_{0\,\mathrm{res}}\frac{\partial \hat{b}_{1m}}{\partial y} \tag{31}$$

is shown in Figs. 14c and 14d. The analogous plot of the buoyancy flux $\hat{B}_1$ is in Figs. 14e and 14f. Comparison of the amplitudes of these terms indicates that the (three-dimensional component of) air–sea buoyancy flux (B_1) is largely balanced by the meridional advection (T_v). The T_u term, whose amplitude is only a third of (and whose phase is significantly shifted relative to) T_v, plays but a minor role in the mixed layer budget.

Term T_v consists of two distinct terms: advection of the zero-order buoyancy by the perturbation of the meridional velocity

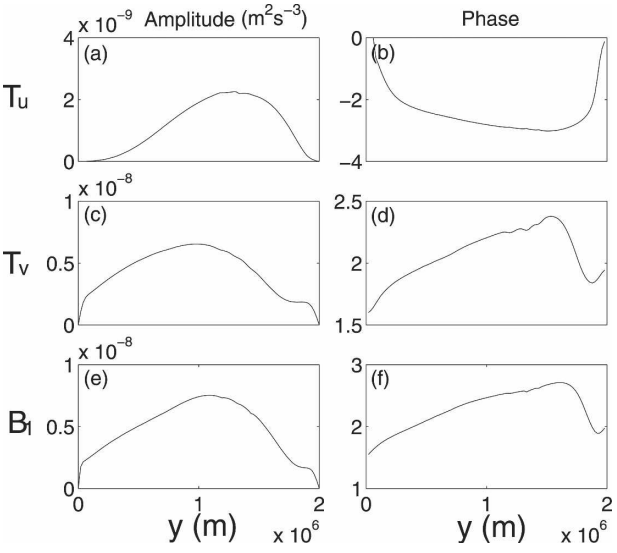

FIG. 14. The (left) amplitudes and (right) phases of the individual three-dimensional (the first Fourier harmonic) components of the mixed layer buoyancy budget in (B12): (a), (b) the zonal advection of buoyancy in (30); (c), (d) the meridional advection of buoyancy in (31); and (e), (f) the air–sea buoyancy flux.

$$T_{v1} = \psi_{1\,\mathrm{res}} \frac{\partial b_{0m}}{\partial y}$$

and advection of the buoyancy perturbation by the zero-order flow

$$T_{v2} = \Psi_{0\,\mathrm{res}} \frac{\partial \hat{b}_{1m}}{\partial y}.$$

Of these two terms, the dominant contribution comes from T_{v1}, and therefore the buoyancy budget of the mixed layer can be approximated by

$$\psi_{1\,\mathrm{res}} \frac{\partial b_{0m}}{\partial y} \approx \hat{B}_1. \tag{32}$$

The balance in (32) suggests that the 3D component of the overturning circulation, as measured by $\psi_{1\,\mathrm{res}}$ immediately below the mixed layer, is largely in phase with the buoyancy forcing. The situation, however, becomes markedly different in the interior of the ACC, where the explicit buoyancy forcing vanishes and stratification comes into play. The buoyancy budget at $O(\varepsilon)$—see (17)—now consists of three distinct terms representing the effects of the advection of buoyancy by the individual components of residual velocity. Unlike the mixed layer budget, the interior dynamics does not reduce to a simple quasi-two-dimensional balance. All three advection terms have comparable amplitudes: their rms values are, correspondingly, $(ub_x)|_{1\mathrm{mode}} = 3.5 \times 10^{-12}\ \mathrm{m\,s^{-3}}$, $(vb_y)|_{1\mathrm{mode}} = 3.8 \times 10^{-12}\ \mathrm{m\,s^{-3}}$, and $(wb_z)|_{1\mathrm{mode}} = 4.8 \times 10^{-12}\ \mathrm{m\,s^{-3}}$. Inspection of the spatial distribution of these terms (not shown) indicates that the zonal advection plays a critical role in the warm upper equatorward regions characterized by swift currents; however, the ub_x term greatly weakens at depth near the base of the model thermocline. These findings indicate that fundamentally three-dimensional effects resulting from the zonal convergence of buoyancy fluxes play a significant role in determining the interior structure of the thermocline.

b. Diabatic eddy fluxes in the mixed layer

Another aspect of our theory, which can be examined by diagnosing the steady-state solution in section 5, is related to the diabatic eddy fluxes and their role in the dynamics of the ACC. In constructing our model, we assumed (section 3) that the eddy transfer is largely adiabatic; that is, the eddy fluxes are directed along the isopycnal surfaces. Since this assumption was based on the two-dimensional model (MR), it becomes necessary now to validate it by using our three-dimensional solution.

Theoretical reasoning and numerical simulation (e.g., Karsten et al. 2002) suggest that the significant diabatic effects of eddies may occur in near-surface frontal regions; presence of the ocean surface tends to suppress the vertical component of the eddy fluxes and thereby forces eddy fluxes to become nearly horizontal in regions where eddies "feel" the surface. As a result, eddy fluxes become directed across the isopycnals, causing significant diapycnal volume fluxes. Thus, in estimating the role of diabatic eddy effects we focus primarily of the near-surface mixed layer.

As discussed in appendix A, the eddy fluxes can be separated into the components parallel and normal to the mean b surfaces. For convenience, in the earlier discussion (section 3) the small diabatic component in (A2)

$$F_{\mathrm{dia}} = \frac{\overline{\mathbf{v}'b'} \cdot \nabla b}{|\nabla b|^2} \nabla b \tag{33}$$

was combined with the explicit buoyancy forcing. Now we directly compute the diabatic term (33) by diagnosing the solution in section 5 and, thus, determine the partitioning of the total flux in the mixed layer ($\tilde{B}$) between the air–sea fluxes (B) and diabatic eddies (B^*).

Equation (33) can be greatly simplified by using the long-wave approximation $\partial/\partial x \ll \partial/\partial y$ and assuming that b_z vanishes in the mixed layer:

$$\nabla F_{\mathrm{dia}} \approx \frac{\partial}{\partial y} \overline{v'b'}. \tag{34}$$

Because the mixed layer is assumed to be vertically homogeneous, the eddy fluxes in (34) are evaluated by applying the interior closure (A8) immediately below the mixed layer and assuming that $\overline{v'b'}$ is vertically uniform within the mixed layer. The total buoyancy flux supplied by air–sea fluxes and the diabatic eddies in the mixed layer reduces to

$$\tilde{B} = B + h_m k_0 \frac{\partial}{\partial y} \left(\left| \frac{b_y}{b_z} \right| b_y \right) \Bigg|_{z=-h_m}. \tag{35}$$

The partitioning of terms in (35) is given in Table 1, which shows that the contribution of the diabatic eddy

TABLE 1. Root-mean-square of the buoyancy fluxes in the mixed layer. First column shows the partitioning of the total buoyancy flux ($\tilde{B}$) between direct air–sea fluxes and diabatic eddy fluxes. The second column presents the partitioning of terms in the first Fourier component of (35).

	Total ($\mathrm{m^2\,s^{-3}}$)	Mode 1 ($\mathrm{m^2\,s^{-3}}$)
Eddy flux (B^*)	6.2×10^{-10}	3.2×10^{-10}
Air–sea flux (B)	6.7×10^{-9}	3.9×10^{-9}

fluxes in the mixed layer budget is an order of magnitude less than the direct air–sea buoyancy flux.[4] The limited significance of the diabatic eddies is seen in the total mixed layer buoyancy budget (the first column in Table 1) and in the first Fourier component of the fluxes as well (the second column in Table 1).

7. Conclusions

A model for the large-scale three-dimensional structure of the Antarctic Circumpolar Current has been presented that assumes that the eddy transport in the interior of the ACC is entirely adiabatic; the diapycnal flux by small-scale turbulence is limited to the upper mixed layer. Tractability is achieved by expressing the buoyancy field in terms of the Fourier series in the zonal direction and drastically truncating the expansion. Our representation consists of only two modes: the dominant streamline average component and the first (fundamental) Fourier harmonic. Accordingly, the model is driven by the two lowest spectral components ($n = 0, 1$ harmonics) of the wind stress and buoyancy forcing.

The new theoretical framework makes it possible to determine the three-dimensional distribution of buoyancy and residual circulation for various surface and boundary conditions. In one of the examples (section 4) we prescribe the surface buoyancy distribution and the air–sea flux and compute the interior fields. However the "prognostic" model in section 5 computes the buoyancy fluxes as a part of the problem, assuming that the stratification at the equatorward flank of the ACC is controlled by the circulation in the adjacent gyres and therefore is regarded as known; results of the two models are mutually consistent. Of particular significance is the ability of the prognostic model to independently predict the amplitude and distribution of the air–sea buoyancy fluxes, which are consistent with observations.

The model solutions represent a balance between the Eulerian meridional overturning, parameterized eddies, and the downstream advection of buoyancy by the mean flow. The latter component is absent in the zonal-average theories of the ACC (e.g., MR) and plays a significant role in determining the three-dimensional structure of the model thermocline. The diabatic eddy effects, on the other hand, are shown (section 6) to be of secondary importance for both streamline-averaged and three-dimensional components of the residual circulation.

Residual circulation in the model is characterized by intensification of the overturning circulation in the Atlantic–Indian Ocean sectors and dramatic reduction in its strength in the Pacific region, a pattern that is readily understood by considering the phases of the surface heat flux and the wind stress. Likewise, the model thermocline is relatively warm, stratified, and deep in the region corresponding to 120°E–60°W. These model predictions are consistent with the hydrography of the Southern Ocean.

Acknowledgments. The support of the Office of Polar Programs of the National Science Foundation is gratefully acknowledged. We thank Taka Ito for help with the analysis of the observed surface forcing fields in the Southern Ocean.

APPENDIX A

Eddy-Induced Velocities of the Residual-Mean Theory

Following Andrews and McIntyre (1976) (see also Plumb and Ferrari 2005; Ferreira et al. 2005), we write the time-mean buoyancy budget (2) as

$$\mathbf{v} \cdot \nabla b = -\nabla \cdot \mathbf{F} + \frac{\partial B}{\partial z}, \tag{A1}$$

where b is the mean buoyancy and the eddy buoyancy flux

$$F = \overline{\mathbf{v}'b'} = \frac{\overline{\mathbf{v}'b'} \cdot \nabla b}{|\nabla b|^2} \nabla b - \frac{\overline{\mathbf{v}'b'} \times \nabla b}{|\nabla b|^2} \times \nabla b \tag{A2}$$

is separated into components parallel and normal to the mean b surfaces. We are mostly concerned here with the second term in (A2), the "skew flux," which is equivalent to advection of b by the following eddy-induced velocity field:

$$\mathbf{v}^* = \nabla \times \phi, \tag{A3}$$

where

$$\phi = -\frac{\overline{\mathbf{v}'b'} \times \nabla b}{|\nabla b|^2}. \tag{A4}$$

[4] A reviewer pointed out that the diabatic eddy flux may be critical for other aspects of the ACC dynamics, particularly in communicating the heating signal downward from the surface and thus increasing the downstream variation in buoyancy.

The first term in (A2) is zero for adiabatic eddies in which the eddy buoyancy fluxes are directed along mean buoyancy surfaces. If, however, eddies have a component normal to b contours, it is convenient (see MR) to combine the diabatic term with the direct diapycnal buoyancy flux (B) by rewriting (A1) as

$$\mathbf{v}_{\text{res}} \cdot \nabla b = \frac{\partial \tilde{B}}{\partial z}, \tag{A5}$$

where $\tilde{B} = B + B^*$ includes a contribution from the diapycnal component of eddy fluxes (B^*). Residual velocities in (A5) are given by

$$\mathbf{v}_{\text{res}} = \mathbf{v} + \mathbf{v}^*.$$

Next, we note that the expression for the eddy velocities in (A3) and (A4) greatly simplifies if the lateral scales significantly exceed the vertical scale ($\partial/\partial z \gg \partial/\partial x$, $\partial/\partial y$), a condition that is generally well satisfied in the ocean (except in the relatively thin surface and bottom mixed layers). In this case, the horizontal eddy velocities reduce to the familiar forms

$$u^* = \frac{\partial}{\partial z}\left(\frac{\overline{u'b'}}{b_z}\right) \quad \text{and}$$
$$v^* = \frac{\partial}{\partial z}\left(\frac{\overline{v'b'}}{b_z}\right). \tag{A6}$$

We adopt a conventional downgradient closure for the eddy buoyancy fluxes in (A6):

$$\overline{u'b'} = -Kb_x, \tag{A7}$$

where the eddy transfer coefficient K is not constant, but rather is determined by the local properties of the flow field. Marshall and Radko (2003) used a model in which K is proportional to the isopycnal slope, a closure suggested by Visbeck et al. (1997) and supported by the laboratory experiments in Cenedese et al. (2004). Extending this model for three-dimensional flows, we assume that

$$\overline{u'b'} = -k_0|s_x|b_x = -k_0\left|\frac{b_x}{b_z}\right|b_x \quad \text{and}$$
$$\overline{v'b'} = -k_0|s_y|b_y = -k_0\left|\frac{b_y}{b_z}\right|b_y, \tag{A8}$$

where k_0 is a positive constant. Parameterization in (A8) reduces (A6) to

$$u^* = -k_0\frac{\partial}{\partial z}(s_x|s_x|) \quad \text{and}$$
$$v^* = -k_0\frac{\partial}{\partial z}(s_y|s_y|). \tag{A9}$$

Eddy-induced velocities can be expressed in terms of the vector streamfunction $\Psi^* = (\Psi_u^*, \Psi_v^*)$ such that $(\partial/\partial z)(\Psi_u^*, \Psi_v^*) = -(u^*, v^*)$, and using (A9) we identify

$$\Psi_u^* = k_0 s_x|s_x| \quad \text{and}$$
$$\Psi_v^* = k_0 s_y|s_y| \tag{A10}$$

for the interior of the ocean below the mixed layer ($z < -h_m$).

In the mixed layer ($-h_m < z < 0$) where isopycnals become vertical, (A10) does not apply. Instead, we require there that $\boldsymbol{\Psi}^*$ varies continuously from a finite value at $z = -h_m$ to zero at the surface ($z = 0$). Therefore, for both the interior and the mixed layer, we can relate the eddy streamfunction and the eddy-induced velocities as follows:

$$\boldsymbol{\Psi}_u^* = -\int_0^z u^*\,dz,$$
$$\boldsymbol{\Psi}_v^* = -\int_0^z v^*\,dz, \quad \text{and}$$
$$w^* = \nabla_h \cdot \boldsymbol{\Psi}^*,$$

providing a consistent model for the nondivergent eddy-induced velocity field whose vertical component (w^*) vanishes at the surface.

APPENDIX B

Reduction of the First-Order Problem to a System of Ordinary Differential Equations

Following MR, we consider separately the adiabatic interior ($z < -h_m$) and a thin, vertically homogeneous mixed layer ($-h_m < z < 0$); see Fig. 3 of MR.

a. Interior dynamics

Since the buoyancy forcing B is assumed to be negligible in the interior, the $O(\varepsilon)$ buoyancy equation in (17), written in terms of $\psi_{1\,\text{res}}$, reduces to

$$J(\psi_{1\,\text{res}}, b_0) + J(\Psi_{0\,\text{res}}, \hat{b}_1) = ik\left(\int_0^z \hat{u}_1 dz\,\frac{\partial b_0}{\partial z} - u_0\hat{b}_1\right), \quad z < -h_m, \tag{B1}$$

where (19) and (20) were used to eliminate $(\hat{w}_{1\,\text{res}}, \hat{v}_{1\,\text{res}})$.

The explicit expression for ψ_1^* is obtained by expanding v^* in powers of ε:

$$\int_0^z v^*\,dz = k_0 s_y^2 = k_0 \frac{\left(\frac{\partial}{\partial y} b\right)^2}{\left(\frac{\partial}{\partial z} b\right)^2} = k_0 \left\{ \frac{b_{0z}^2}{b_{0y}^2} + \mathrm{Re}\left[2\frac{b_{0y}}{b_{0z}^3} (\hat{b}_{1y} b_{0z} - \hat{b}_{1z} b_{0y}) \exp(ikx) \right] + O(\varepsilon^2) \right\}. \tag{B2}$$

Therefore, isolating the first-order ($\sim\varepsilon$) term, we find

$$\psi_1^* = -2k_0 \frac{b_{0y}}{b_{0z}^3} J(\hat{b}_1, b_0). \tag{B3}$$

The first-order y-momentum equation written in terms of $\psi_{1\ \mathrm{res}}$ is

$$f\frac{\partial \psi_{1\ \mathrm{res}}}{\partial z} = -ik\hat{P}_1 + f\frac{\partial \psi_1^*}{\partial z} + \frac{\partial \hat{\tau}_{1x}}{\partial z}. \tag{B4}$$

Integrating (B4) once in z and recalling that $\psi_1^*|_{z=0} = \psi_{1\ \mathrm{res}}|_{z=0} = 0$, we arrive at

$$f\psi_{1\ \mathrm{res}} = -ik\int_0^z \hat{P}_1\,dz + f\psi_1^* - \hat{\tau}_{1x}|_{z=0}. \tag{B5}$$

Despite the seemingly complicated form of the governing equations in (B1) and (B5), they can be efficiently integrated along the "old," zero-order characteristics. For the characteristic velocities (v_c, w_c) given by (16),

$$\begin{aligned} \frac{d}{dl}(\cdot) &\equiv v_c \frac{\partial}{\partial y}(\cdot) + w_c \frac{\partial}{\partial z}(\cdot) = \frac{\partial}{\partial y}(\cdot) + s_0 \frac{\partial}{\partial z}(\cdot) \\ &= \frac{1}{b_{0z}} J(\cdot, b_0), \end{aligned} \tag{B6}$$

and therefore the first term in the buoyancy equation in (B1) reduces to $b_{0z} d\psi_{1\ \mathrm{res}}/dl$. Likewise, using (B6) we simplify the second term on the left-hand side of (B1) to

$$\begin{aligned} J(\Psi_{0\mathrm{res}}, \hat{b}_1) &= -\left(\frac{d\Psi_{0\ \mathrm{res}}}{db_0}\right) J(\hat{b}_1, b_0) \\ &= -b_{0z}\left(\frac{d\Psi_{0\ \mathrm{res}}}{db_0}\right)\frac{d\hat{b}_1}{dl}, \end{aligned} \tag{B7}$$

and thus (B1) reduces to

$$\frac{d\psi_{1\ \mathrm{res}}}{dl} - \left(\frac{d\Psi_{0\ \mathrm{res}}}{db_0}\right)\frac{d\hat{b}_1}{dl} + ik\frac{u_0 \hat{b}_1}{b_{0z}} = ik\int_0^z \hat{u}_1\,dz. \tag{B8}$$

The momentum equation in (B5) can also be greatly simplified by expressing it in terms of the (zero order) isentropic gradients. Using (B6), we rewrite (B3) as

$$\psi_1^* = 2k_0 \frac{s_0}{b_{0z}} \frac{d\hat{b}_1}{dl}. \tag{B9}$$

Substituting ψ_1^* given by (B9) into (B5), we arrive at

$$\frac{d\hat{b}_1}{dl} - \frac{(\psi_{1\mathrm{res}} + \tau_{1x}/f) b_{0z}}{2k_0 s_0} = ik\frac{b_{0z}\int_0^z \hat{P}_1\,dz}{2k_0 s_0 f}. \tag{B10}$$

b. Mixed layer

The steady, vertically homogeneous, mixed layer buoyancy budget in 3D is

$$u_{\mathrm{res}}\frac{\partial b_m}{\partial x} + v_{\mathrm{res}}\frac{\partial b_m}{\partial y} = \frac{\partial B}{\partial z}. \tag{B11}$$

To proceed with the truncated spectral model, (B11) is integrated in z over the depth of the mixed layer h_m, and the result is expanded in powers of ε using (8). The first-order ($\sim\varepsilon$) component is given by

$$iku_0 \hat{b}_{1m} h_m + \psi_{1\mathrm{res}}\frac{\partial b_{0m}}{\partial y} + \Psi_{0\mathrm{res}}\frac{\partial \hat{b}_{1m}}{\partial y} = \hat{B}_1, \tag{B12}$$

where $\Psi_{0\ res}$, $\psi_{1\ \mathrm{res}}$ are evaluated at the bottom of the mixed layer, resulting in an explicit expression for $\psi_{1\ \mathrm{res}}|_{z=-hm}$

$$\psi_{1\ \mathrm{res}} = \frac{\hat{B}_1 - \Psi_{0\ \mathrm{res}}|_{z=-h_m}\frac{\partial}{\partial y}\hat{b}_{1m} - iku_0\hat{b}_{1m}h_m}{\frac{\partial}{\partial y} b_{0m}}. \tag{B13}$$

Equations in (B8), (B10), and the surface boundary condition (B13) are used in the model (sections 4 and 5) to efficiently compute the steady three-dimensional components of buoyancy and residual circulation of the ACC.

REFERENCES

Andrews, D. G., and M. E. McIntyre, 1976: Planetary waves in horizontal and vertical shear: The generalized Eliassen–Palm flux and the mean zonal acceleration. *J. Atmos. Sci.,* **33,** 2031–2049.

Cenedese, C., J. Marshall, and J. A. Whitehead, 2004: A laboratory model of thermocline depth and exchange fluxes across circumpolar fronts. *J. Phys. Oceanogr.,* **34,** 656–667.

Ferreira, D., J. Marshall, and P. Heimbach, 2005: Estimating eddy

stresses by fitting dynamics to observations using a residual-mean ocean circulation model and its adjoint. *J. Phys. Oceanogr.,* **35,** 1891–1910.

Held, I. M., 1983: Stationary and quasi-stationary eddies in the extratropical troposphere: Theory. *Large-scale Dynamical Processes in the Atmosphere.* B. J. Hoskins and R. P. Pearce, Eds., Academic Press, 127–199.

Johnson, G. C., and H. L. Bryden, 1989: On the size of the Antarctic Circumpolar Current. *Deep-Sea Res.,* **36,** 39–53.

Karsten, R., and J. Marshall, 2002a: Testing theories of the vertical stratification of the ACC against observations. *Dyn. Atmos. Oceans,* **36,** 233–246.

——, and ——, 2002b: Constructing the residual circulation of the ACC from the observations. *J. Phys. Oceanogr.,* **32,** 3315–3327.

——, H. Jones, and J. Marshall, 2002: The role of eddy transfer in setting the stratification and transport of a circumpolar current. *J. Phys. Oceanogr.,* **32,** 39–54.

Kuo, A., R. A. Plumb, and J. Marshall, 2005: Transformed Eulerian-mean theory. Part II: Potential vorticity homogenization and the equilibrium of the wind- and buoyancy-driven zonal flow. *J. Phys. Oceanogr.,* **35,** 175–187.

Luyten, J., J. Pedlosky, and H. Stommel, 1983: The ventilated thermocline. *J. Phys. Oceanogr.,* **13,** 292–309.

Marshall, D., 1995: Topographic steering of the Antarctic Circumpolar Current. *J. Phys. Oceanogr.,* **25,** 1636–1650.

Marshall, J., and T. Radko, 2003: Residual-mean solutions for the Antarctic Circumpolar Current and its associated overturning circulation. *J. Phys. Oceanogr.,* **33,** 2341–2354.

——, D. Olbers, H. Ross, and D. Wolf-Gladrow, 1993: Potential vorticity constraints on the dynamics and hydrography of the Southern Ocean. *J. Phys. Oceanogr.,* **23,** 465–487.

Plumb, A. R., and R. Ferrari, 2005: Transformed Eulerian-mean theory. Part I: Nonquasigeostrophic theory for eddies on a zonal-mean flow. *J. Phys. Oceanogr.,* **35,** 165–174.

Rhines, P. B., and W. R. Young, 1982: A theory of the wind-driven circulation I: Mid-ocean gyres. *J. Mar. Res.,* **40** (Suppl.), 559–596.

Rintoul, S. R., C. W. Hughes, and D. Olbers, 2001: The Antarctic Circumpolar Current system. *Ocean Circulation and Climate,* G. Siedler, J. Church, and J. Gould, Eds., International Geophysics Series, Vol. 77, Academic Press, 271–302.

Sun, C., and D. R. Watts, 2002: Heat flux carried by the Antarctic Circumpolar Current mean flow. *J. Geophys. Res.,* **107,** 3119, doi:10.1029/2001JC001187.

Visbeck, M., J. Marshall, T. Haine, and M. Spall, 1997: Specification of eddy transfer coefficients in coarse-resolution ocean circulation models. *J. Phys. Oceanogr.,* **27,** 381–402.